Ag-doped TiO_2 with Tuneable Ag^0 and Ag^+ for Enhanced Photocatalytic Degradation of RR4 Dye

Nureel Imanina Abdul Ghani, Nur Izzati Nabilah Zanal, Nadiah Sabihah Md Natar, Siti Raihan Hamzah, Muhammad Afiq Rosli, Nur Aien Muhamad, Mohammad Saifulddin Mohd Azami, Sarina Mohamad and Wan Izhan Nawawi Wan Ismail*

Faculty of Applied Sciences, Universiti Teknologi MARA (UiTM), 02600 Arau, Perlis, Malaysia

*Corresponding author (e-mail: wi_nawawi@uitm.edu.my)

This study proposed to enhance the photocatalytic performance of Ag-TiO_2 by manipulating Ag^0 and Ag^+ formation on TiO_2 through controlled dissolved oxygen (DO) levels by photo-deposition of Ag (1-5 wt.%) to TiO_2 under N_2 gas purging (0-60 min; denoted as DO^0-DO^{60}). The photocatalytic performance of the immobilised Ag-TiO_2 was determined under the photodegradation of Reactive Red 4 (RR4) dye. XRD and FTIR revealed the existence of Ag^+ and Ag^0, corresponding to Ag_2O and Ag-TiO_2, respectively. The HRTEM images showed a spheroid shape of Ag-TiO_2 with 0.20 and 0.24 nm of d-spacing, representing Ag metal and Ag_2O, respectively. The lower PL intensity of Ag-TiO_2 suggested a reduced e^-/h^+ recombination rate, while UV-Vis/DRS analysis indicated strong visible light absorption due to the surface plasmonic resonance (SPR) effect. This study proves that Ag_2O can increase photocatalytic performance as an electron injector to Ag-TiO_2, however, excess formation of Ag_2O can retard the photocatalytic activity. Optimal 3 wt.% Ag doping at 30 min N_2 purging (3AT-DO^{30}) achieved complete 30 mg L^{-1} RR4 dye degradation in 1 hour, surpassing unmodified TiO_2 by 63.1%. The photocatalytic performance order was TiO_2 < 3AT-DO^{60} < 3AT-DO^0 < 3AT-DO^{10} < 3AT-DO^{30}, with all samples maintaining stability over 10 cycles.

Keywords: Dissolved oxygen; RR4 dye; silver; titanium dioxide; wastewater

Received: July 2023; Accepted: November 2023

Wastewater management has become a concern these days due to the inability to treat effluents properly. Wastewater may contain hazardous materials such as toxic chemicals, heavy metals, dyes, and organic compounds [1]. Industries such as printing factories and textile manufacturers heavily use dye in their production. This event will lead to the accumulation of dye in water bodies. Nearly 10,000 different synthetic dyes can be found in the market, and over 700,000 tons are produced annually worldwide. Almost 200,000 tons of synthetic dyes are released into the mainstream because of the ineffective dyeing method used in textile industries [2]. Reactive Red 4 (RR4) is one of the anionic dyes commonly used in the printing and textile industry [3]. This monoclorotriazin dye has a high molecular weight and contains four sulfonate groups [4]. RR4 dye also contains a hydrophobic molecule that is soluble in aqueous media, although some anionic dyes are toxic and carcinogenic to living things [5].

Several technologies have been proposed for wastewater treatment such as adsorption, photo-Fenton process, ozonation, and electrochemical filtration. Advanced oxidation process (AOP), such as photo-catalysis is one of the techniques that shows strong potential for the effective removal of dye pollutants in wastewater [6]. This process involves semiconductors and production of hydroxyl radicals as the main oxidant to oxidise model pollutants [7]. Photocatalysis produces no secondary wastes and is readily available and easily accessible, despite it only needing a low cost to operate [8]. These advantages have received extensive attention from researchers.

Titanium dioxide (TiO_2) is a good semiconductor due to its non-toxicity, stability, availability, photo-chemically active, and low cost [9, 10]. However, TiO_2 can only be activated by irradiation of UV light (5% of sunlight) due to its relatively large band gap energy, which is 3.2 eV [11]. The fast electron-hole (e^-/h^+) recombination of TiO_2 also becomes a drawback in photocatalytic performance [12]. To overcome these problems, researchers have modified TiO_2 by doping with noble metals such as platinum (Pt) [13], silver (Ag) [14], and gold (Au) [15]. Doping with noble metals will reduce the band gap energy and extend the absorption of TiO_2 into the visible light spectrum [16].

Silver (Ag) has been extensively used to enhance the photocatalytic performance of TiO_2 due to the surface plasmonic resonance (SPR) effect. When light strikes the semiconductor, Ag will create traps to capture the photogenerated electrons, leading to the formation of metallic silver, Ag^0 on the surface of TiO_2 [14]. This phenomenon will reduce the electron-

hole (e^-/h^+) recombination rate and enhance the photocatalytic performance of TiO_2. Modification of TiO_2 with Ag has been an effective solution to overcome the limitations of TiO_2 semiconductors due to its non-toxicity, relatively low cost compared with other metals such as Pt, and its special behaviour of oxygen adsorption [17]. Jinhui *et al.* prepared immobilised Ag/TiO_2 with cellulose-derived carbon beads as the carrier via the One-Pot method to remove ceftriaxone sodium; an antibiotic pollutant in waste-water [18]. Grieken *et al.* reported that immobilised Ag/TiO_2 in a catalytic wall reactor showed better degradation of *Escherichia coli* compared to a fixed-bed reactor [19]. Besides, Ag/TiO_2 immobilised on rotating vanes prepared by Pariya *et al.* showed outstanding performance for leachate post-treatment where it removed 62% COD and 55% TOC after 4 h irradiation [20]. Zunaira *et al.* evaluated the growth of *Bacillus subtilis* and *Escherichia coli* with immobilised Ag-TiO_2 coated onto a polyamide nano-filtration membrane. The results showed approximately 75% and 73% of reduced bacterial growth for *Escherichia coli* and *Bacillus subtilis*, respectively [21].

However, the preparation of Ag-TiO_2 commonly results in the generation of Ag and Ag_2O in the composite, which is unfavourable for the photocatalytic reaction, thus reducing photocatalytic performance [22]. This phenomenon is associated with the presence of dissolved oxygen (DO) in water that can easily re-oxidise the reduced metal [23]. The presence of DO in the photocatalytic reduction system will limit the reduction of metal on TiO_2 as metal needs to compete with oxygen for photo-yielded electrons, e^- [24]. Wang *et al.* have proved that reduction of U(VI) on TiO_2 semiconductors would not happen in the presence of oxygen. Nevertheless, with the use of 2-propanol as a sacrificial agent, the efficiency of the deposition of U(VI) on TiO_2 remained high even in the presence of oxygen, but still lower than in the N_2 condition [25]. In addition, the ability of sacrificial agents to affect the oxidation state and the dispersion of the metal deposited has been claimed by Vaelma and Selin [26]. They claim that a lower concentration of a sacrificial agent will produce a metal with a higher oxidation state, such as Pt^{II} or Pt^{IV}, while a higher sacrificial agent concentration can produce metallic Pt^0. Moreover, the sacrificial agent also will scavenge the holes from the photocatalyst by donating electrons to the TiO_2 lattice. When a smaller number of holes are present, the photogenerated electrons can easily participate in metal-reducing reactions because they are less likely to recombine. Therefore, a sacrificial reagent is used in the photocatalytic system to facilitate the reduction of $AgNO_3$ (Ag^+) into metallic Ag (Ag^0).

To the best of our knowledge, there is no previous study that has been conducted in the modification of immobilised TiO_2 with Ag with the control of Ag_2O formation during the preparation steps. Thus, in this study, the preparation of Ag-TiO_2 with the elimination of DO was conducted by bubbling with N_2 gas for 0, 10, 30, and 60 min, with isopropyl alcohol (IPA) as a sacrificial reagent. The photocatalytic degradation ability of water-based preparation of immobilised Ag-TiO_2 was tested under the photodegradation of RR4 dye.

EXPERIMENTAL

Chemicals and Materials

All the reagents were of analytical grade and used as received without further purification. TiO_2 used is a commercially available Degussa P25 (ca. 80% anatase, 20% rutile, BET surface area of 50 $m^2\ g^{-1}$ and average particle size of 25 nm). Silver nitrate ($AgNO_3$) as an Ag precursor, isopropyl alcohol (IPA) as a sacrificial agent, and polyvinyl alcohol (PVA) as a polymer binder were all purchased from Sigma-Aldrich. Reactive Red 4 (RR4) dye (also known as Cibacron Brilliant Red, purity: 50% dye content, λ max: 517) was used as a model pollutant and purchased from Aldrich Chemical. Double-sided adhesive tape (DSAT) was purchased from the local store. Laboratory distilled water was used throughout this experiment.

Preparation of Ag-TiO_2 with Controlled DO

Silver nitrate was used as an Ag precursor to enhance the photocatalytic activity of commercially available TiO_2. The preparation of the Ag-TiO_2 photocatalyst was according to the method by Bhardwaj *et al.* with slight modifications [14]. For this method, 0.0478 g of $AgNO_3$ (corresponding to 1 wt.% Ag-TiO_2) was dissolved in 40 mL of 50% IPA solution. For 3 and 5 wt.% Ag-TiO_2, the amount of $AgNO_3$ used was 0.1461 g and 0.2487 g, respectively. Then, 3 g of TiO_2 was added to the solution and magnetically stirred until homogenised. The mixture was soaked for 5 h before undergoing the photodeposition process. After soaking time, the mixture of Ag-TiO_2 was transferred into a Schlenk tube and sealed properly. Nitrogen gas was purged into the Schlenk tube to remove any excess oxygen. For the dissolved oxygen (DO) study, the DO of the optimum percentage of Ag-TiO_2 was manipulated by N_2 gas purging with a long needle into the mixture to remove DO at a controlled time (denoted as DO^x, x = 0, 10, 30, and 60 min). A portable multi-meter (HACH HQ4300, United States) was used to measure the amount of dissolved oxygen in the mixture. The photodeposition of Ag-TiO_2 took place by irradiating the mixture with a 250 W metal halide lamp (LIKO, Malaysia) for an hour. After irradiation time, the mixture was filtered using vacuum filtration and washed 3 times with distilled water. The obtained Ag-TiO_2 was dried for 15 h at room temperature. The dried sample was ground and stored in an amber vial until further usage.

For the control study, Ag_2O was prepared to compare its effect on the photodegradation of RR4

dye. To produce Ag_2O, an aliquot of 20 mL of $AgNO_3$ and 20 mL of NaOH was mixed in a test tube. A brown precipitate formed as the chemicals mixed, indicating a successful formation of Ag_2O. After the dull brown clump of Ag_2O settled at the bottom of the test tube, the liquid $NaNO_3$ was removed. The Ag_2O was dried with a low flame to remove any remaining moisture.

Immobilisation of Ag-TiO_2

Ag-TiO_2 was immobilised by a DSAT method using a brush coating technique as was introduced by Wan Ismail *et al.* [5]. 0.5 g of powdered Ag-TiO_2 plus 1 mL of 8% PVA were mixed with 10 mL of distilled water and sonicated with an ultrasonicator (Crest Ultrasonics, New Jersey, model: 4HT-1014-6, amps: 6) until homogenised. Ag-TiO_2 was applied to the glass plate taped with DSAT (area of 4.6 cm x 3 cm) via brush coating and was dried using a hot air blower. The photocatalyst was applied layer by layer until the optimum weight of the coating was reached [27]. The excess coating and impurities on the finished Ag- TiO_2 plate were removed with a washing process with distilled water for 30 min.

Photocatalytic Degradation of RR4 Dye

The photocatalytic activity of the prepared Ag-TiO_2 was determined by the photodegradation of RR4 dye. For the suspension mode, an aliquot of 20 mL of RR4 dye (30 mg L^{-1}) and 0.025 g of Ag-TiO_2 were mixed by sonication, before being placed in a glass cell (L × W × H: 5 × 10 × 8 cm). Before the 55 W fluorescence lamp was turned on for the photodegradation process, the suspension was aerated in dark conditions to achieve a complete adsorption/desorption equilibrium. An aliquot of 3 ml was taken from the suspension using a syringe and filtered using a membrane filter before the absorbance reading was taken. The photo-degradation took place for 20 min and the absorbance reading was taken at every 5 min interval at a wavelength of 517 nm with a spectrophotometer (HACH DR1900, United States). The procedure of photodegradation of RR4 dye by immobilised Ag-TiO_2 was the same as the suspension mode except without a separation process. An aliquot of 7 mL of the RR4 dye was poured into a glass cell before placing the immobilised Ag-TiO_2. A different time interval of 15 min for absorbance reading was applied. After measuring the absorbance, the treated dye was dispensed back into the glass cell to continue the photodegradation process. Figure 1 illustrates the photocatalysis setup utilised for the immobilised mode. The degradation rate of RR4 dye was calculated using the Langmuir-Hinshelwood model formula as in Equation (1) [28].

$$\ln \frac{C}{C_0} = -k_{app}\, t \qquad (1)$$

Where C is the current concentration, C_0 represents the initial concentration, and t is time.

Characterisation

The characterisation performed included Fourier Transform Infrared (FTIR, PerkinElmer Frontier, USA) with ACD/Spectrus Processor 2020.2.0 software to analyse various functional groups contained in the Ag-TiO_2 photocatalyst in the range of 400-4000 cm^{-1}. X-ray diffraction (XRD, D5000 Bruker, Germany) with X-ray energy Cu-Kα (1.54 A°) at 45 kV in diffraction range, 2θ of 20–80° was used to detect the crystallographic characteristics of the modified Ag-TiO_2 High-Resolution Transmission Electron Microscopy (HRTEM, JEM- 2100F JEOL, Japan) was used to study the lattice fringes of the Ag-TiO_2 photocatalyst. Photo-luminescence spectroscopy (PL, HR-800 HORIBA, Japan) was used to detect the reduction of electron-hole recombination of the Ag-TiO_2 photocatalyst. UV-Vis Diffuse Reflectance Spectroscopy (DRS, Perkin Elmer Lambda 35, USA) with a range of 200-800 nm

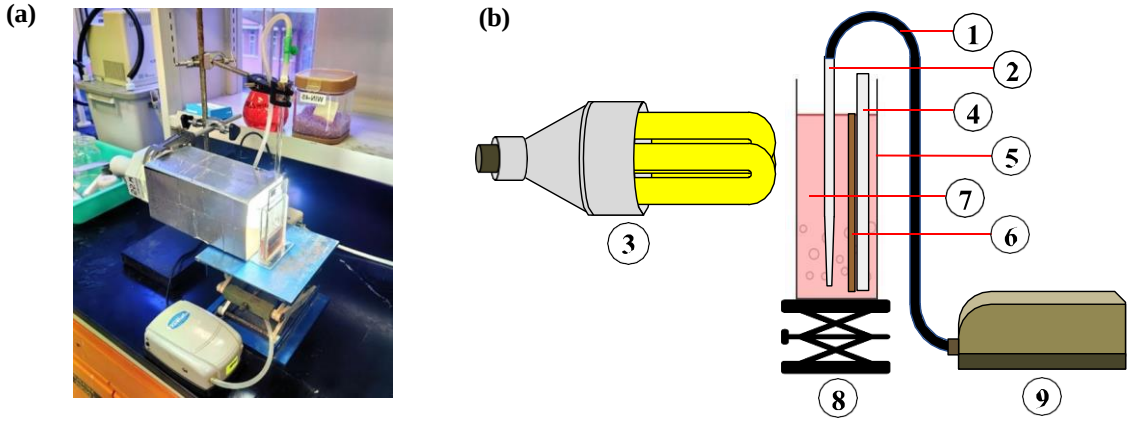

Figure 1. (a) Real and (b) illustrated photocatalysis setup for the photodegradation of RR4 dye. Labels represent: (1) aeration tube; (2) pasteur pipette; (3) lamp; (4) glass plate;(5) glass cell; (6) Ag-TiO_2 coating; (7) RR4 dye; (8) scissor jack; and (9) pump.

was used to determine the band gap of the Ag-TiO_2 samples. The colour changes of the prepared samples were determined by physical observation.

RESULTS AND DISCUSSION

Characterisation of Ag-TiO_2

The summary of the prepared unmodified TiO_2 and Ag-TiO_2 samples is allocated in Table 1, which the first order rate constant indicates the photocatalyst performance for the degradation of RR4 dye. The colour variations of the unmodified TiO_2, Ag-TiO_2, and Ag_2O are shown in Figure 2. The difference in the colour of the Ag-TiO_2 photocatalysts (Figures 2(b-e)) indicates the successful incorporation of Ag metal into the TiO_2 lattice. While Ag_2O (Figure 2(f)) appeared dark brown [29], Ag-TiO_2 looked more toned down in different shades of purple.A parallel observation was reported by Albiter *et al.* on the preparation of Ag-TiO_2, which highlighted that the $AgNO_3$ precursor can produce a photocatalyst with a certain shade of purple [30]. This can be explained through the specific charge transfer transition ($T_{2g} \rightarrow E_g$) between Ag and TiO_2. The colour changes from white to different shades of purple with decreasing DO, indicating that there were notable reactions that happen by altering the amount of DO in the mixture prior to photodeposition. This phenomenon might happen due to less formation of Ag_2O with decreasing DO content. From 3AT-DO^0 (Figure 2(b)) to 3AT-DO^{60} (Figure 2(e)), the colour intensity of the photocatalyst decreased. Compared to pure Ag_2O in Figure 2(f) which has a dark brown colour, the appearance of 3AT-DO^{60} can be attributed to the reduced or lack of formation of Ag_2O between the Ag-TiO_2 photocatalyst. Thus, successful doping of silver into TiO_2 could be observed through the colour changes of the samples.

Table 1. Experimental conditions and first-order rate constant of Ag-TiO_2 samples in suspension and immobilised modes.

Sample	Loading of Ag (wt.%)	N_2 gas purging time (min)	DO conc. (mg/L)	1st order rate constant (min^{-1})	
				Suspension	Immobilised
TiO_2	-	0	9.63	0.079	0.041
1AT	1.0	0	9.62	0.080	0.049
3AT	3.0	0	9.60	0.109	0.058
5AT	5.0	0	9.61	0.091	0.051
3AT-DO^{10}	3.0	10	5.08	0.123	0.085
3AT-DO^{30}	3.0	30	1.52	0.156	0.112
3AT-DO^{60}	3.0	60	0.96	0.071	0.048

*3AT is equal to 3AT-DO^0

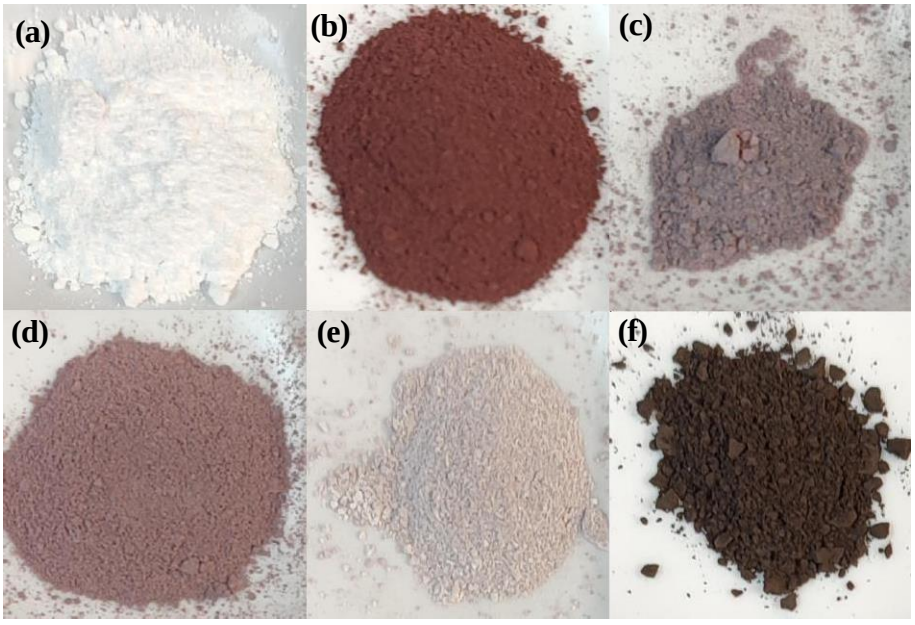

Figure 2. Colour intensity of (a) unmodified TiO_2, (b-e) 3AT-DO^0 to 3AT-DO^{60}, and (f)Ag_2O.

Table 2. FTIR peaks and corresponding functional groups

FTIR peak (cm^{-1})	Functional group assigned
3428, 1627	stretching and bending vibration of hydroxyl group (OH)
537	stretching vibration of Ag-O
655, 1400	lattice vibration of unmodified TiO_2 (Ti-O-Ti stretching)
1384	lattice vibration of Ag-TiO_2 (Ti-O-Ag stretching)

The FTIR spectra of Ag_2O, unmodified TiO_2, and 3AT-DO^0 to 3AT-DO^{60} samples are illustrated in Figure 3(a). Broad peaks present at 3428 cm^{-1} and 1627 cm^{-1} represent the stretching and bending vibration of the hydroxyl group (OH) due to the water molecule absorbed on the catalyst surface [31]. Kunnamareddy *et al.* stated that OH^- absorbed performs an important role in photocatalysis as it captures photoinduced charge carriers to generate reactive OH radicals, which then degrade organic pollutants [32]. The stretching vibration of Ag-O is assigned to the peak near 537 cm^{-1} [33]. The peaks observed in the unmodified TiO_2 sample at 655 cm^{-1} and near 1400 cm^{-1} are attributed to the lattice vibration of TiO_2 (Ti-O-Ti stretching) [34]. With the addition of 3 wt.% Ag, the peak for TiO_2 lattice vibration was observed to shift from 1400 cm^{-1} to 1384 cm^{-1}, which suggests the formation of Ag-TiO_2 bonding. Table 2 exhibits the peaks obtained from the FTIR analysis and the equivalent functional groups.

The crystal structures of unmodified TiO_2, 3AT-DO^0 until 3AT-DO^{60}, and Ag_2O were investigated using XRD analysis in the range of 2θ = 20-80°, as shown in Figure 3(b). All the diffraction peaks of the samples can be indexed to the anatase phase of TiO_2 (JCPDS Card: 01- 078-2486). Several peaks of Ag-TiO_2 were observed at 2θ = 25.307°, 37.792°,48.043°, 53.886°, 55.068°, 62.689°, and 68.756°, and indexed as (101), (004), (200), (105), (211), (204), and (116), respectively. A previous study by You *et al.* had shown peaks for Ag metal (Ag^0) observed at 2θ = 37.8° (004) and 44.3° (200), which could also be seen in our sample [35]. This proves that Ag particles were successfully incorporated into the TiO_2 lattice. For 3AT-DO^0 until 3AT-DO^{60} samples, a clear peak could be observed at 32.468° (111), which is assigned to Ag_2O particles. As the bubbling time increased from 0 min to 60 min, the intensity of the peak became weaker due to the less amount of dissolved oxygen in the sample that will react with Ag^0 to form Ag_2O particles.

The band gap energy of the unmodified and Ag-modified TiO_2 was investigated via UV/vis diffuse reflectance spectroscopy, as shown in Figures 3(c) and (d). The calculated Kubelka-Munk function is shown in Equation (2) [29].

$$F(R) = \frac{(1-R)^2}{2R} \quad (2)$$

Where *F(R)* is the Kubelka-Munk function and *R* is reflectance.

Unmodified TiO_2 with a white colour, exhibited an absorption band at λ = 380 nm, which is consistent with the intrinsic band gap of anatase TiO_2 of 3.2 eV calculated from the formula λ = 1240 / Ebg; where λ is the incident wavelength in nm, 1240 is the Planck's constant, and Ebg is the obtained band gap energy [36]. Compared to the unmodified TiO_2, the Ag-TiO_2 samples presented a strong visible light absorption. This is due to their intense colour which exhibited absorption owing to surface plasmon oscillations of the Ag metal [37].

The band gap energies of 1AT, 3AT, and 5AT determined from the intercepts were 2.5, 2.2, and 2.85 eV, respectively. The narrow band gaps could be attributed to the Schottky barrier formed at the interface of Ag metal and TiO_2. This barrier that forms at metal-semiconductor junctions can trap electrons, causing the accumulation of electrons at Ag nanoparticles. Thus, the band gap energy of Ag-TiO_2 will be decreased as the Fermi level becomes closer to the conduction band of TiO_2 [38]. 3AT depicted the lowest band gap among the modified photocatalysts, suggesting its easier photoexcitation by incident light of lower energy and its capability of photocatalytic enhancement under visible irradiation.

For Ag_2O, the dark brown sample showed an absorption of more than 380 nm, corresponding to the p-type semiconductor with a band gap of 1.2 eV [39]. Although Ag_2O has a low band gap and was reported to be applicable as a strong decolouring agent in the photocatalytic activity over organic pollutants [40], it is unstable under experimental conditions [36], thus making it not efficient as a photocatalyst. Another study mentioned that silver oxidation in the hetero-structure changes the metal-semiconductor interface and causes plasmonic enhancement suppression [41].

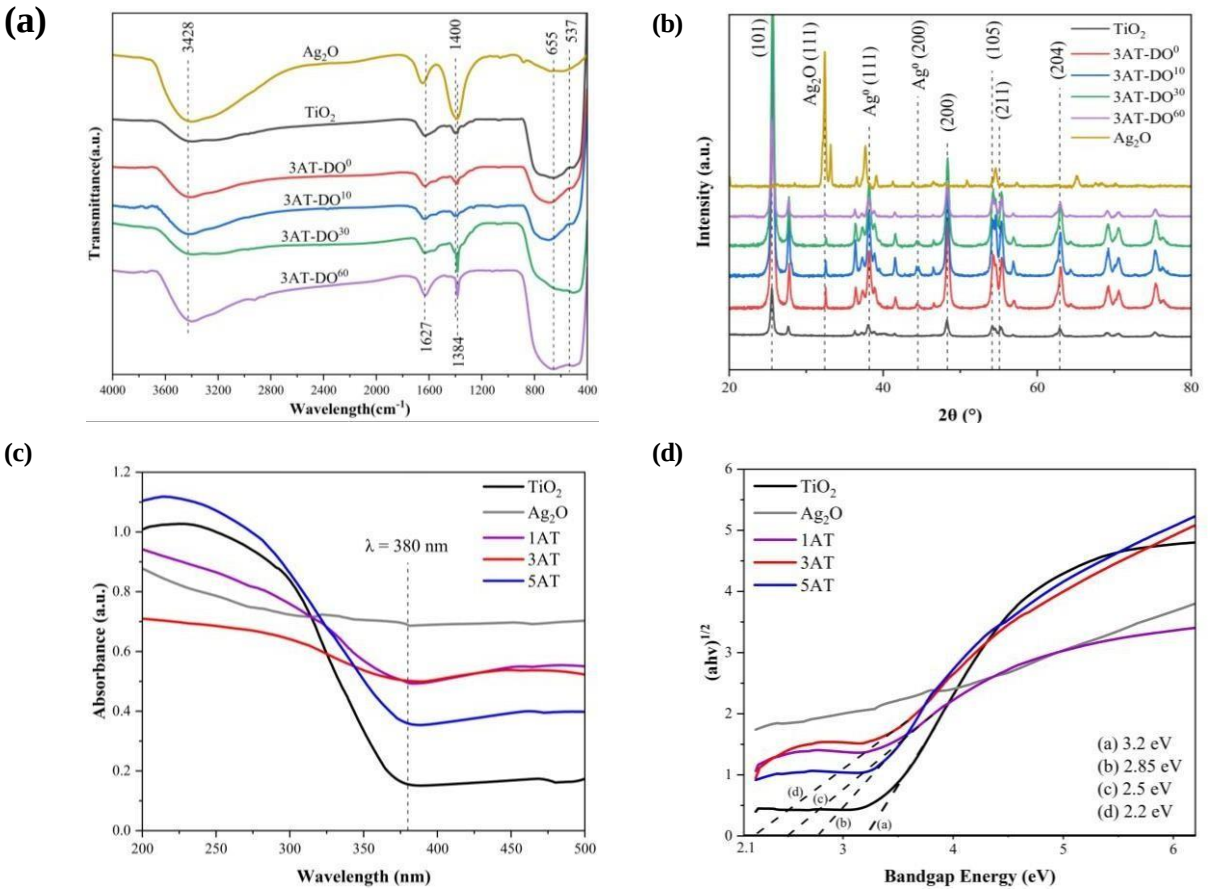

Figure 3. (a) FTIR spectra and (b) XRD analysis of Ag_2O, unmodified TiO_2 and 3AT-DO^0 to 3AT-DO^{60}; and (c) UV/vis spectra and (d) band gaps of unmodified TiO_2 and Ag-TiO_2 with various Ag contents.

The movement and separation of e^-/h^+ pairs are essential in determining the photocatalytic performance of a photocatalyst. According to Komaraiah *et al.*, luminescence emission is considered a surface phenomenon that might be caused by the de-excitation of electrons from their excitation state to the ground state with decreasing light energy [42]. Since photo-luminescence (PL) emission is attributed to the recombination of photogenerated charge carriers, this analysis is often used to verify the separation efficacy of e^-/h^+ pairs in a photocatalyst [17]. In Figure 4, the PL spectra of Ag-modified TiO_2 are presented, both for the percentage of Ag loading (Figure 4(a)) and the effect of dissolved oxygen (Figure 4(b)).

From Figure 4(a), it can observed that 3AT had the lowest PL signal intensity compared to 1AT and 5AT, with the highest peak detected at 548 nm. This suggests that 3AT has a better separation of photogenerated charge carriers among other loadings of Ag, thus 3AT was selected as an optimum sample for the DO study. In Figure 4(b), it is illustrated that the DO-manipulated 3AT photocatalysts had lower emissions compared to the unmodified TiO_2. Both phenomena in Figures 4(a) and (b) indicate that the deposition of Ag successfully minimised the recombination rate of e^-/h^+ under UV and visible light exposure [38]. Several excitation peaks were observed at 392, 472, 504, 508, and 520 nm for TiO_2. Notably, the intense peak at 392 nm is attributed to both direct and indirect transitions in the titania phase (anatase and rutile) of TiO_2. Whereas the peaks at 472, 504, 508, and 520 nm reflect the recombination by surface traps due to oxygen and hydroxyl defects [43].

For Ag-modified samples, it is worth mentioning that 3AT-DO^0 and 3AT-DO^{60} had quite similar emission peaks, whilst there were sudden decrements for 3AT-DO^{10} and 3AT-DO^{30}. As the amount of DO reflects on the Ag_2O production, it is safe to state that 3AT-DO^0 had the highest amount of Ag_2O, whereas 3AT-DO^{60} was the lowest or none. From the PL peak, it is suggested that the Ag_2O within the Ag-TiO_2 samples (as verified by XRD) can act as an electron scavenger, thereby more charge separation. However, the amount of Ag_2O in the samples needs to be optimal, as too much or too little can result in e^-/h^+ separation inefficiency. For 3AT-DO^{30}, the Ag presented in metallic form was much higher compared to the others, which means that more oxide forms of Ag have been converted to zero states (Ag^0), resulting in better charge separation and thus low PL intensity.

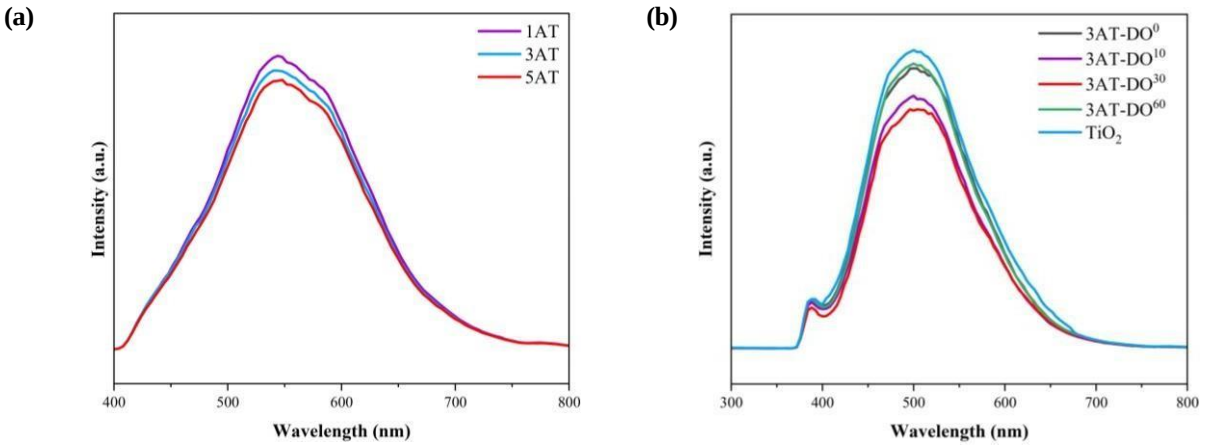

Figure 4. PL spectra for (a) 1AT, 3AT and 5AT, and (b) TiO_2 and 3AT-DO^0 to 3AT-DO^{60} of Ag-TiO_2.

Figure 5 shows the HRTEM images of the Ag-TiO_2 photocatalyst, exhibiting a population of Ag nanoparticles (dark particles) on the TiO_2 surface. In Figure 5(a), the HRTEM images confirm that Ag-TiO_2 are in spheroid shape and Ag nanoparticles have high distribution on the surface of TiO_2. In Figure 5(b), the images reveal the presence of the anatase phase indexed as (101), identified by spacing d = 0.3659 nm [30]. Figure 5(c) displays the deposit of Ag^0 on TiO_2 detected by spacing d = 0.2034 nm and indexed as (200). In Figure 5(d), the HRTEM micrographs exhibit the composite material formed by Ag_2O, indexed as (002) with spacing d = 0.24 nm. From the HRTEM images, it is confirmed that there was the formation of both Ag_2O and Ag^0 in the Ag-TiO_2, which can affect the photocatalytic efficiency of the photocatalyst under anionic RR4 dye degradation.

Photocatalytic Performance

The photocatalytic efficiency of the Ag-TiO_2 samples was evaluated under photodegradation of 30 mg/L RR4 dye under visible light irradiation. From the results obtained, it is revealed that the photocatalytic activity in the suspension mode exceeded the immobilised mode, as shown in Figures 6(a) and (b). Nevertheless, the photocatalytic reaction in the immobilised mode was comparable to the suspension mode, as mentioned by Wan Ismail *et al.* [5]. From Figure 6(c), it can be seen that all k-values of the modified TiO_2 surpassed the pure TiO_2, except for 3AT-DO^{60}. Based on Table 1, less amount of dissolved oxygen was present in 3AT-DO^{60}, thus we can claim that there was less formation of Ag_2O in the sample. Although the presence of Ag_2O in the sample could retard the photocatalytic performance, the absence of Ag_2O could also reduce its efficiency as Ag_2O can act as an e^- injector in assisting the photodegradation of the dye.

The increment trend of the photocatalytic reaction could be observed from 3AT-DO^0 until 3AT-DO^{30} with the k-value 0.1087 to 0.1562 for the suspension mode, while for the immobilised mode, the k-value increased from 0.0584 to 0.1116. The k-value of the photocatalyst represents the % degradation of the dye. The higher the k-value, the higher the percentage degradation. The highest photocatalytic efficiency could be seen in 3AT-DO^{30}, which could be attributed to the efficient e^-/h^+ pair separation and low band gap energy. The higher the wt.% loading of Ag, the better the photocatalytic performance until an optimum is reached. For the dissolved oxygen study, lower dissolved oxygen will produce a higher photodegradation rate until a maximum is attained. As for the difference between suspension and immobilised modes, the suspension mode surpasses the immobilised mode due to the higher surface-to-volume ratio. Nevertheless, our immobilised mode results show comparable photocatalytic activity against the suspension mode.

Most metal oxides such as TiO_2 are amphoteric and can react as both acid and base [44].

The reaction equation can be described as follows (Equations (3) and (4)):

$$MOH \leftrightarrow MO^- + H^+ \quad (3)$$

$$MOH \leftrightarrow M^+ + OH^- \quad (4)$$

Where M represents the solid surface of metal oxide.

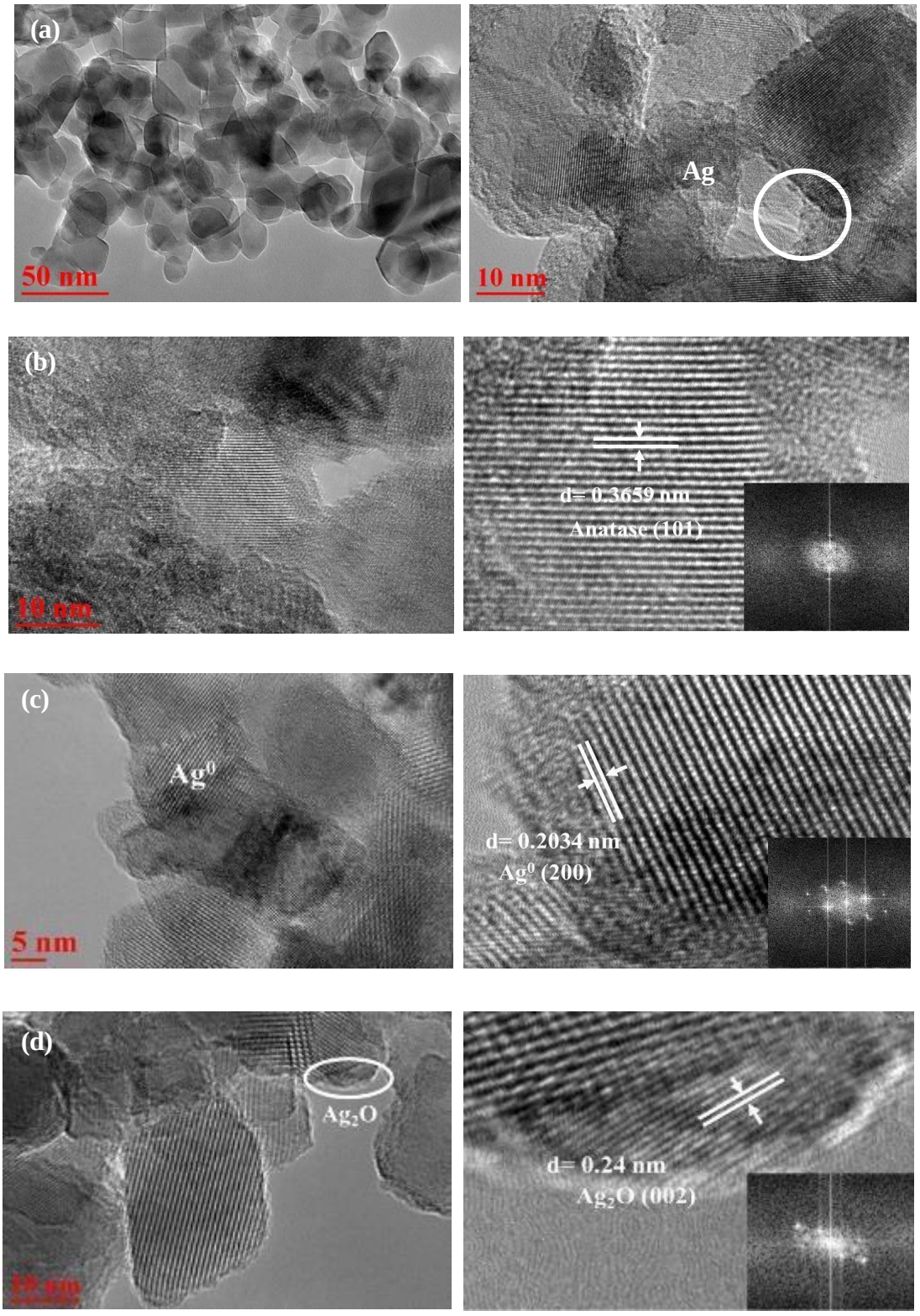

Figure 5. HRTEM images of (a) Ag-TiO_2 nanocrystals showing a population of metallic silver(Ag^0) and Ag_2O on the TiO_2 support, (b) anatase TiO_2, (c) metallic silver (Ag^0), and (d) Ag_2O.

The adsorption efficiency of dye molecules to the Ag-TiO_2 photocatalyst which can facilitate the photodegradation can be determined by the point of zero charges (PZC) of the photocatalyst. PZC is the pH of the suspension where the net charge on the surface of the photocatalyst is zero [45]. Based on Figure 6(d), it can be seen that the point of zero charges of the photocatalyst was at pH 6.3. In an acidic environment, a TiO_2-based photocatalyst will be protonated, since pH < pH_{PZC}; while in an

alkaline environment, pH > pH_{PZC}, causes TiO_2 to be deprotonated. Considering RR4 dye as an anionic dye, the absorption of the dye on TiO_2 is easier in an acidic environment due to a powerful electrostatic attraction between the negatively charged dye molecule and the positively charged surface of Ag-TiO_2 [46]. The mechanisms of the reaction can be described as follows (Equations (5) and (6)):

$$pH < pH_{PZC} : TiOH + H^+ \rightarrow TiOH_2^+ \quad (5)$$

$$pH > pH_{PZC} : TiOH + OH^- \rightarrow TiO^- + H_2O \quad (6)$$

From the perspective of Ag_2O formation in the samples, it can be assumed that the formation of Ag_2O did reduce the photocatalytic reaction, however insufficient or zero amount of Ag_2O would result in a decreased reaction. As stated by Albiter *et al.*, Ag_2O can act as a light harvester which can transfer electrons from their conduction band mainly to surface silver nanoparticles and avoid charge recombination, thus producing higher photocatalytic activity [30]. Table 2 summarises the corresponding first-order rate constant that highlights the superiority of the 3AT-DO^{30} sample, which exhibited excellent photocatalytic degradation among all samples.

To evaluate the stability and reusability of the Ag-TiO_2 samples, the photodegradation of RR4 dye was repeated for 10 consecutive cycles. Figure 7 depicts the performance of the Ag-TiO_2 samples, where all the samples tested exhibit stable photocatalytic activity and reusability without catalyst leaching. The highest photocatalytic activity was displayed by 3AT- DO^{30} at the 3rd cycle, which gradually decreased by the 10 th cycle. The great sustainability of the Ag-TiO_2 samples was due to the strong attachment of the photocatalyst to the glass support material facilitated by the DSAT binder. It also can be assumed that the sustained photocatalytic performance of the photocatalysts is ascribed to the solid intermolecular attraction between Ag and TiO_2, where they cannot be easily separated [47]. In summary, Ag-TiO_2 is feasible for reusability, with high photo-degradation up to 10 cycles.

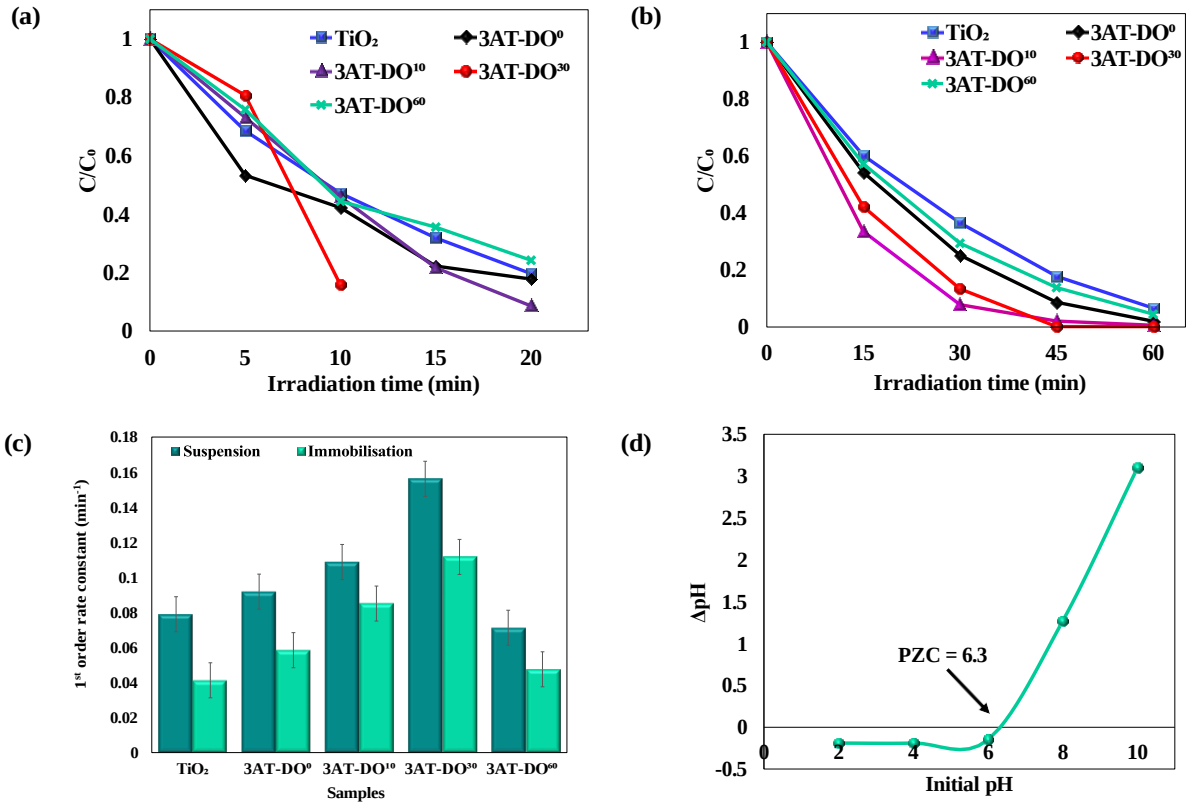

Figure 6. (a-b) Photodegradation of RR4 dye in suspension and immobilised modes shown as C/C0, (c) first-order rate constant (k) values of TiO_2 and Ag-TiO_2 samples, and (d) point of zero charges for 3AT-DO^{30} photocatalyst.

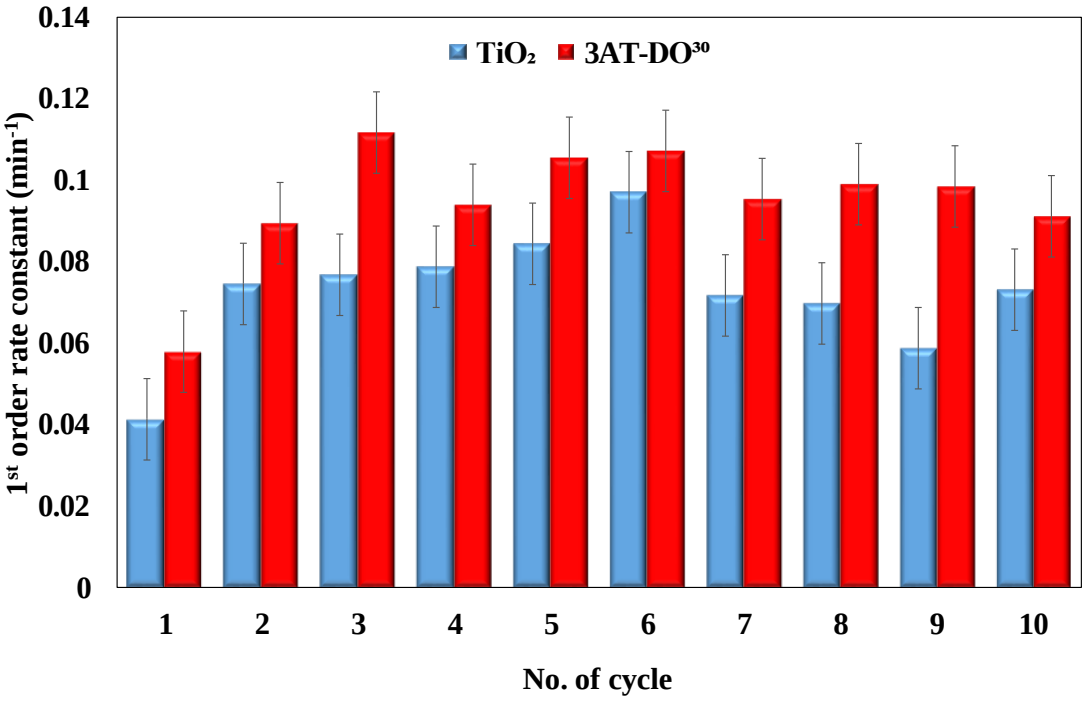

Figure 7. Photocatalytic performance of Ag-TiO_2 samples under 1 h visible lightirradiation upon 10 continuous cycles.

Proposed Mechanism of Modified TiO_2

Figure 8 shows the photocatalytic mechanism pathway of Ag-TiO_2 for the photodegradation of RR4 dye under visible light illumination based on several characterisations such as UV-vis/DRS, PL, and XRD analyses. When the TiO_2 semiconductor is exposed to light irradiation, thus having equivalent energy or more than the band gap energy of TiO_2, electrons in the valence band become excited and move to the conduction band, leaving behind holes in the valence band (Eq. (7)). The photogenerated electrons and holes (e^-/h^+) produced play an important role in the photodegradation process. Doping TiO_2 with Ag has been proved through PL analysis to reduce the recombination rate of (e^-/h^+) pairs. This is due to the Schottky barrier effect, in which Ag particles become attached to the TiO_2 semiconductor to obtain Fermi-level equilibration that leads to the generation of monovalent Ag [48]. Metallic Ag (Ag^0) formed, that was observed through XRD analysis, helps to reduce the band gap energy through interactions between TiO_2-Ag phases by trapping the photo-generated electrons to the Ag clusters, where it will reduce the chances for (e^-/h^+) recombination, thus enhancing the photocatalytic performance [49]. In the presence of N_2 gas (Figure 8(a)), e^-/h^+ generated will react with oxygen and water-producing superoxide anion (O_2^-•) and hydroxyl radicals (OH•) respectively (Equations (8) and (9)). However, without N_2 gas purging (Figure 8(b)), Ag particles may react with dissolved oxygen in water and generate Ag_2O, which gives a lower catalytic performance (Equation (11)). This is due to oxygen molecules poisoning Ag by occupying the active sites of Ag particles. The concentration of oxygen leads to the same degree of poisoning, which means that a higher amount of dissolved oxygen will give a higher rate of catalyst poisoning, thus lower photocatalytic efficiency [50]. In addition, DO also acts as an electron scavenger, which is a competition reaction with the reduction of Ag^+ that affects the photocatalytic rate [27]. Therefore, the presence of N_2 gas is crucial to inhibit the formation of Ag_2O which leads to catalyst poisoning. The reactive oxygen species (ROS) formed such as O_2^-• and OH• will degrade RR4 dye into harmless products, which are CO_2 and H_2O. The mechanisms of the reaction can be described as follows:

$$Ag : TiO_2 + h\nu \rightarrow Ag : TiO_2\ (h^+_{vb} + e^-_{cb}) \quad (7)$$

$$H_2O/OH^- + h^+_{vb} \rightarrow OH\bullet \quad (8)$$

$$e^-_{cb} + O_2\ (ads) \rightarrow O^-_2 \quad (9)$$

$$AgNO_3 + H_2O \rightarrow Ag^+ + NO_3^- \quad (10)$$

$$AgNO_3 + O_2 \rightarrow Ag_2O + 4NO_3 \quad (11)$$

$$Ag^+ + h^+_{vb} \rightarrow Ag^{2+} \quad (12)$$

$$Ag^{2+} + H_2O\ /OH^- \rightarrow OH\bullet + Ag^+ \quad (13)$$

$$Ag^+ + e^-_{cb} \qquad Ag^0 \quad (14)$$

$$Ag^0 + O_2\ (ads) \rightarrow Ag^+ + O^-_2 \quad (15)$$

$$Ag^0 + Ti^{4+} \rightarrow Ag^+ + Ti^{3+} \quad (16)$$

$$Ti^{3+} + O_2\ (ads) \rightarrow Ti^{4+} + O^-_2 \quad (17)$$

$$O^-_2 + h^+_{VB} \rightarrow O^- \quad (18)$$

$$O^- + H_2O\ (ads) \rightarrow OH\bullet + OH^- \quad (19)$$

$$R + OH\bullet \rightarrow R'' + H_2O + CO_2 \quad (20)$$

(a)

(b)

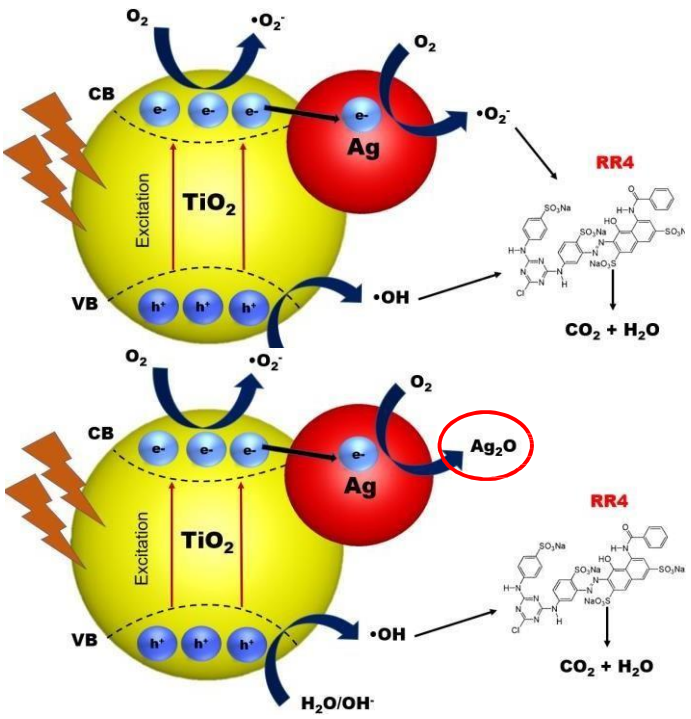

Figure 8. Schematic diagrams of the proposed mechanism of Ag-TiO_2 (a) in the presence of N_2 gas and (b) without N_2 gas purging.

Abbreviation list	
AOP	Advanced oxidation process
BET	Brunauer-Emmett Teller
ca.	*circa* (about; around)
COD	Chemical oxygen demand
DO	Dissolved oxygen
DSAT	Double-sided adhesive tape
e^-/h^+	Electron-hole
eV	Electron volt
FTIR	Fourier transformer infrared
HRTEM	High-resolution transmission electron microscopy
IPA	Isopropyl alcohol
PL	Photoluminescence
PVA	Polyvinyl alcohol
PZC	Point zero charge
ROS	Reactive oxygen species
RR4	Reactive Red 4
SPR	Surface plasmonic resonance
TOC	Total organic carbon
UV-Vis/DRS	Ultraviolet-visible diffuse reflectance spectroscopy
W	Watt
XRD	X-ray diffraction

CONCLUSION

In summary, the formation of Ag_2O on the Ag-TiO_2 photocatalyst was successfully controlled by manipulating the amount of DO in the mixture during preparation prior to photodeposition. Significantly, the presence of Ag_2O in the photocatalyst reflects the photocatalytic performance of Ag-TiO_2 in the photodegradation of the anionic RR4 dye. The formation of Ag^0 and Ag_2O needs to be in sufficient amounts, as too much or too little may result in low photocatalytic performance. The results confirm that the deposition of Ag on TiO_2 extends the absorption into the visible light spectrum and reduces the e^-/h^+ recombination rate. The high dispersion of Ag nanoparticles onto the TiO_2 surface without agglomeration ensures a balanced photocatalytic reaction. The descending order of photocatalytic performance of Ag-TiO_2 was as follows: 3AT-DO^{30} > 3AT-DO^{10} > 3AT-DO^0 > 3AT-DO^{60} > TiO_2, and all samples exhibited stable photocatalytic performance upon 10 cycles. This work investigated the effect of Ag_2O on the photocatalytic performance of Ag-TiO_2, providing excellent insights into producing a powerful photo-catalyst for the degradation of organic contaminants.

DECLARATION OF COMPETING INTERESTS

The authors declare that they have no known competing financial interests or personal relationships that could have appeared to influence the work reported in this paper.

ACKNOWLEDGMENT

We would like to express our gratitude to Universiti Teknologi MARA (UiTM) for providing a generous internal financial support of this study under GIP 2022/2 grant: RMC/RD/47/006/2023 and for all the facilities.

REFERENCES

1. Saravanan, A., Kumar, P. S., Jeevanantham, S., Karishma, S., Tajsabreen, B., Yaashikaa, P. R. & Reshma, B. (2021) Effective water/wastewater treatment methodologies for toxic pollutants removal: Processes and applications towards sustainable development. *Chemosphere*, **280**, 130595.

2. Al-Mamun, M. R., Kader, S., Islam, M. S., & Khan, M. Z. H. (2019) Photocatalytic activity improvement and application of UV-TiO_2 photocatalysis in textile wastewater treatment: A review. *Journal of Environmental Chemical Engineering*, **7(5)**, 103248.

3. Azami, M. S., Ismail, K., Ishak, M. A. M., Zuliahani, A., Hamzah, S. R., & Nawawi, W. I. (2020) Formation of an amorphous carbon nitride/titania composite for photocatalytic degradation of RR4 dye. *Journal of Water Process Engineering*, **35**, 101209.

4. Hoffmann, S., Fuenzalida Werner, J. P., Moreno-Villoslada, I., & Goycoolea, F. M. (2016) New

insights into the nature of the Cibacron brilliant red 3B-A–Chitosan interaction. *Pure and Applied Chemistry*, **88(9)**, 891–904.

5. Wan Ismail, W. I. N., Ain, S. K., Zaharudin, R., Jawad, A. H., Ishak, M. A. M., Ismail, K., & Sahid, S. (2015) New TiO_2/DSAT immobilization system for photodegradation of anionic and cationic dyes. *International Journal of Photoenergy*, **2015**.

6. Natarajan, S., Bajaj, H. C., & Tayade, R. J. (2018) Recent advances based on the synergetic effect of adsorption for removal of dyes from waste water using photocatalytic process. *Journal of Environmental Sciences*, **65**, 201–222.

7. Nosaka, Y., & Nosaka, A. (2016) Understanding hydroxyl radical (• OH) generation processes in photocatalysis. *ACS Energy Letters*, **1(2)**, 356–359.

8. Al-Nuaim, M. A., Alwasiti, A. A., & Shnain, Z. Y. (2023) The photocatalytic process in the treatment of polluted water. *Chemical Papers*, **77(2)**, 677–701.

9. Lu, Z., Zhou, H. F., Liao, J. J., Yang, Y. Y., Wang, K., Che, L. M., He, N., Chen, X. D., Song, R., Cai, W. F., Liu, H., & Wu, X. E. (2019) A facile dopamine-assisted method for the preparation of antibacterial surfaces based on Ag/TiO_2 nanoparticles. *Applied Surface Science*, **481**, 1270–1276.

10. Dharma, H. N. C., Jaafar, J., Widiastuti, N., Matsuyama, H., Rajabsadeh, S., Othman, M. H. D., Rahman, M. A., Jafri, N. N. M., Suhaimin, N. S., Nasir, A. M., & Alias, N. H. (2022) A review of titanium dioxide (TiO_2)-based photocatalyst for oilfield-produced water treatment. *Membranes*, **12(3)**, 345.

11. Devipriya, S. P., Yesodharan, S., & Yesodharan, E. P. (2012) Solar photocatalytic removal of chemical and bacterial pollutants from water using Pt/TiO_2-coated ceramic tiles. *International Journal of Photoenergy*, **2012**.

12. Yu, X., Kim, B., & Kim, Y. K. (2013) Highly enhanced photoactivity of anatase TiO_2 nanocrystals by controlled hydrogenation-induced surface defects. *ACS Catalysis*, **3(11)**, 2479–2486.

13. Alamelu, K. & Ali, J. (2018). TiO_2-Pt composite photocatalyst for photodegradation and chemical reduction of recalcitrant organic pollutants. *Journal of environmental chemical engineering*, **6(5)**, 5720–5731.

14. Bhardwaj, S., Sharma, D., Kumari, P. & Pal, B. (2020) Influence of photodeposition time and loading amount of Ag co-catalyst on growth, distribution and photocatalytic properties of Ag@ TiO_2 nanocatalysts. *Optical Materials*, **106**, 109975.

15. Do, T. C. M. V., Nguyen, D. Q., Nguyen, K. T. & Le, P. H. (2019) TiO_2 and Au-TiO_2 nanomaterials for rapid photocatalytic degradation of antibiotic residues in aquaculture wastewater. *Materials*, **12(15)**, 2434.

16. Natar, N. S., Ghani, N. I. A., Hamzah, S. R., Rosli, M. A., Muhamad, N. A., Azami, M. S., Ishak, M. A. M., Razak, S. & Nawawi, W. I. (2022) The Role of Nitrogen-Doped TiO_2 Supported by Platinum Catalyst Synthesized via Various Mode Preparations for Photocatalytic Enhancement. *Nanomaterials*, **12(22**), 3998.

17. Elsellami, L., Dappozze, F., Houas, A. & Guillard, C. (2017) Effect of Ag^+ reduction on the photocatalytic activity of Ag-doped TiO_2. *Superlattices and Microstructures*, **109**, 511–518.

18. Yang, J. & Luo, X. (2021) Ag-doped TiO_2 immobilized cellulose-derived carbon beads: One-Pot preparation, photocatalytic degradation performance and mechanism of ceftriaxone sodium. *Applied Surface Science*, **542**, 148724.

19. Van Grieken, R., Marugán, J., Sordo, C., Martínez, P. & Pablos, C. (2009) Photocatalytic inactivation of bacteria in water using suspended and immobilized silver-TiO_2. *Applied Catalysis B: Environmental*, **93(1-2)**, 112–118.

20. Amigh, P. & Mokhtarani, N. (2022) Leachate post treatment, using Ag-TiO_2 nanoparticles immobilized on rotating vanes. *Journal of Water Process Engineering*, **47**, 102842.

21. Habib, Z., Khan, S. J., Ahmad, N. M., Shahzad, H. M. A., Jamal, Y., & Hashmi, I. (2019) Antibacterial behaviour of surface modified composite polyamide nanofiltration (NF) membrane by immobilizing Ag-doped TiO_2 nanoparticles. *Environmental Technology*, **41(28)**, 3657–3669.

22. Huang, Q., Liu, S., Wei, W., Yan, Q. & Wu, C. (2015) Selective synthesis of different ZnO/Ag nanocomposites as surface enhanced Raman scattering substrates and highly efficient photocatalytic catalysts. *RSC Advances*, **5(34)**, 27075–27081.

23. Li, P., Wang, J., Wang, Y., Liang, J., Pan, D., Qiang, S., & Fan, Q. (2019) An overview and recent progress in the heterogeneous photocatalytic reduction of U (VI). *Journal of Photochemistry and Photobiology C: Photochemistry Reviews*,

41, 100320.

24. Wu, X., Jiang, S., Song, S. & Sun, C. (2018) Constructing effective photocatalytic purification system with P-introduced g-C_3N_4 for elimination of UO_2^{2+}. *Applied Surface Science*, **430**, 371–379.

25. Wang, J., Wang, Y., Wang, W., Peng, T., Liang, J., Li, P., Pan, D., Fan, Q. & Wu, W. (2020) Visible light driven Ti^{3+} self-doped TiO_2 for adsorption-photocatalysis of aqueous U(VI). *Environmental Pollution*, **262**, 114373.

26. Vaelma, M. & Selin, J. (2017) *Photodeposition of Gold and Platinum on Titanium Dioxide*, M.Sc. Thesis, Aalto University, Espoo, Finland.

27. Nawi, M. A. & Wan Ismail, W. I. N. (2013) Preparation and characterization of TiO_2 coated with a thin carbon layer for enhanced photo-catalytic activity under fluorescent lamp and solar light irradiations. *Applied Catalysis A: General*, **453,** 11047.

28. Karthik, P., Ravichandran, S., Sasikala, V., Prakash, N., Mukkannan, A., & Rajesh, J. (2023) Effective photodegradation of organic water pollutants by the facile synthesis of Ag_2O nanoparticles. *Surfaces and Interfaces*, **40**, 103088.

29. Chen, Y. X., Yuan, Y. M., Yang, H. Y., Wang, Q., Ren, Y., Guo, X. H., Zhang, P., Zhang, M. J., Wang, W. & Chu, L. Y. (2023) Hierarchical porous tannic-acid-modified MOFs/alginate particles with synergized adsorption-photocatalysis for water remediation. *Separation and Purification Technology*, **330(B)**, 125435.

30. Albiter, E., Valenzuela, M. A., Alfaro, S., Valverde, A. G. & Martínez-Pallares F. M. (2015) Photocatalytic deposition of Ag nanoparticles on TiO_2: Metal precursor effect on the structural and photoactivity properties. *Journal of Saudi Chemical Society*, **5(19)**, 563–573.

31. Saoud, K., Alsoubaihi, R., Bensalah, N., Bora, T., Bertino, M. & Dutta, J. (2015) Synthesis of supported silver nano-spheres on zinc oxide nano-rods for visible light photocatalytic applications. *Materials Research Bulletin*, **63,** 134–140.

32. Kunnamareddy, M., Diravidamani, B., Rajendran, R., Singaram, B. & Varadharajan, K. (2018) Synthesis of silver and sulphur codoped TiO_2 nanoparticles for photocatalytic degradation of methylene blue. *Journal of Materials Science: Materials in Electronics*, **21(29)**, 18111–18119.

33. Kadam, A., Dhabbe, R., Gophane, A., Sathe, T. & Garadkar, K. (2016) Template free synthesis of ZnO/Ag_2O nanocomposites as a highly efficient visible active photocatalyst for detoxification of methyl orange. *Journal of Photochemistry and Photobiology B: Biology*, **154**, 24–33.

34. Alsharaeh, E. H., Bora, T., Soliman, A., Ahmad, F., Bharath, G., Ghoniem, M. G., Abu K. M. & Dutta, J. (2017) Sol-gel-assisted microwave-derived synthesis of anatase Ag/TiO_2/GO nanohybrids toward efficient visible light phenol degradation. *Catalysts*, **7(5)**, 103390.

35. You, X., Chen, F., Zhang, J. & Anpo, M. (2005) A novel deposition precipitation method for preparation of Ag-loaded titanium dioxide. *Catalysis Letters*, **(102)3**, 247–250.

36. Akel, S., Dillert, R., Balayeva, N. O., Boughaled, R., Koch, J., Azzouzi, M. E. & Bahnemann, D. W. (2018) Ag/Ag_2O as a co-catalyst in TiO_2 photo-catalysis: Effect of the co- catalyst/photocatalyst mass ratio. *Catalysts*, **(8)12**, 647.

37. Shume, W. M., Murthy, H. C. A. & Zereffa, E. A. (2020) A review on synthesis and characterization of Ag_2O nanoparticles for photocatalytic applications. *Journal of Chemistry*, **(2020)**, 5039479.

38. Chen, Y., Ji, S., Chen, C., Peng, Q., Wang, D. & Li, Y. (2018) Single-atom catalysts: synthetic strategies and electrochemical applications. *Joule*, **(2)7**, 1242–1264.

39. Zhang, Z., Hao, H., Yang, H., Zhu, L., Ding, C., Zhang, G., Bi, J., Yan, S., Liu, G. & Hou, H. (2021) UV-Vis-NIR light-driven Ag_2O/Ag_2S/$CuBi_2O_4$ double Z-scheme configuration for enhanced photocatalytic applications. *Materials Science Semiconductor Process*, **126**, 105668.

40. Kumar, Y. K., Gupta, N., Kumar, A., Reece, L. M., Singh, N., Rezania, S. & Khan, S. A. (2018) Mechanistic understanding and holistic approach of phytoremediation: A review on application and future prospects. *Ecological Engineering*, **120**, 274–298.

41. Ziashahabi, A., Prato, M., Dang, Z., Poursalehi, R. & Naseri, N. (2019) The effect of silver oxidation on the photocatalytic activity of Ag/ZnO hybrid plasmonic/metal-oxide nanostructures under visible light and in the dark. *Sci Rep*, **(9)1**, 480757.

42. Komaraiah, D., Radha, E., Kalarikkal, N., Sivakumar, J., Ramana Reddy, M. V. & Sayanna, R. (2019) Structural, optical and photoluminescence studies of sol-gel synthesized pure and iron doped TiO_2 photocatalysts. *Ceramic Inter-*

nationals, **(45)18**, 25060–25068.

43. Chen, W. T., Chan, A., Sun-Waterhouse, D., Moriga, T., Idriss, H. & Waterhouse, G. I. N. (2015) Ni/TiO2: A promising low-cost photocatalytic system for solar H2 production from ethanol-water mixtures. *Journal of Catalysis*, **326,** 43–53.

44. Bi, Z., Li, K., Jiang, C., Zhang, J., Ma, S., Alberto, C., Sun, M., Bu, Y., Barati, M. & Ren, S. (2022) New insights into the traditional charge compensation theory: amphoteric behavior of TiO_2 under the guidance of supply-demand relationship. *ACS Omega*, **(7)24,** 21225–21232.

45. Mahmood, T., Saddique, M. T., Naeem, A., Westerhoff, P., Mustafa, S. & Alum, A. (2011) Comparison of different methods for the point of zero charge determination of NiO. *Industrial & Engineering Chemistry Research*, **(50)17,** 10017–10023.

46. Sun, Q., Hou, P., Wu, S., Yu, L. & Dong, L. (2021) The enhanced photocatalytic activity of Ag-Fe_2O_3-TiO_2 performed in Z-scheme route associated with localized surface plasmon resonance effect. *Colloids and Surfaces A: Physicochemical and Engineering Aspects*, **628**, 127304.

47. Ghani, N. I. A., Rosli, M. A., Hamzah, S. R., Natar, N. S., Nazeri, N. S., Aziz, S. I. A, Mohamad, S., Suhaimi, N. H. S., Adzis, N. S. M. A., Azami, M. S. M. & Wan Ismail, W. I. N. (2022) Water-based immobilized ag-doped TiO_2 photocatalyst for photocatalytic degradation of RR4 dye. *Science Letters*, **(16)2**, 16322.

48. Din, M. I., Khalid, R. & Hussain, Z. (2018) Minireview: Silver-doped titanium dioxide and silver-doped zinc oxide photocatalysts. *Analytical Letters*, **(51)6**, 892–907.

49. Ortiz, A. L., Zaragoza, M. M., Gutiérrez, J. S., Paula, M. D. S. & Collins-Martínez, V. (2015) Silver oxidation state effect on the photocatalytic properties of Ag doped TiO2 for hydrogen production under visible light, *International Journal of Hydrogen Energy*, **(40)48**, 17308–17315.

50. Moghaddam, A. A. & Krewer, U. (2020) Poisoning of ammonia synthesis catalyst considering off-design feed compositions. *Catalysts*, **(10)**, **11**, 1–16.